NMR Analysis of the Monomeric Form of a Mutant Unliganded Bovine Neurophysin: Comparison with the Crystal Structure of a Neurophysin Dimer[†,§]

Tam L. Nguyen[‡] and Esther Breslow*

Department of Biochemistry, Weill Medical College of Cornell University, 1300 York Avenue, New York, New York 10021

Received November 19, 2001; Revised Manuscript Received February 25, 2002

ABSTRACT: Determination of the structure of the unliganded monomeric state of neurophysin is central to an understanding of the allosteric relationship between neurophysin peptide-binding and dimerization. We examined this state by NMR, using the weakly dimerizing H80E mutant of bovine neurophysin-I. The derived structure, to which more than one conformer appeared to contribute, was compared with the crystal structure of the unliganded des 1−6 bovine neurophysin-II dimer. Significant conformational differences between the two proteins were evident in the orientation of the 3,10 helix, in the 50−58 loop, in β-turns, and in specific intrachain contacts between amino- and carboxyl domains. However, both had similar secondary structures, in independent confirmation of earlier circular dichroism studies. Previously suggested interactions between the amino terminus and the 50−58 loop in the monomer were also confirmed. Comparison of the observed differences between the two proteins with demonstrated effects of dimerization on the NMR spectrum of bovine neurophysin-I, and preliminary investigation of the effects of dimerization on H80E spectra, allowed tentative distinction between the contributions of sequence and self-association differences to the difference in conformation. Regions altered by dimerization encompass most binding site residues, providing a potential explanation of differences in binding affinity between the unliganded monomeric and dimeric states. Differences between monomer and dimer states in turns, interdomain contacts, and within the interdomain segment of the 50−58 loop suggest that the effects of dimerization on intrasubunit conformation reflect the need to adjust the relative positions of the interface segments of the two domains for optimal interaction with the adjacent subunit and/or reflect the dual role of some residues as participants both at the interface and in interdomain contacts.

Neurophysins are disulfide-rich carrier proteins for the hormones oxytocin and vasopressin, and are important to the targeting of these hormones to regulated neurosecretory vesicles and their storage in these vesicles (reviewed in ref *1*). Figure 1 shows the primary structures of BNP-I[1] and BNP-II, which share a sequence homology of >75% and closely related properties (*1*). In vivo, oxytocin and vasopressin are bound in 1:1 complexes with BNP-I and BNP-II, respectively, but the two hormones and related peptides bind similarly to both neurophysins in vitro (*1*). Unliganded BNP exists in a monomer−dimer equilibrium that is is strongly driven to dimer by occupancy of the hormone-binding site (*2*) and that is integral to hormone targeting (e.g., ref *1* and *4*); peptide-binding increases the dimerization constant by ∼100 fold (*3*). The mechanism of ligand-facilitated NP dimerization is unclear.

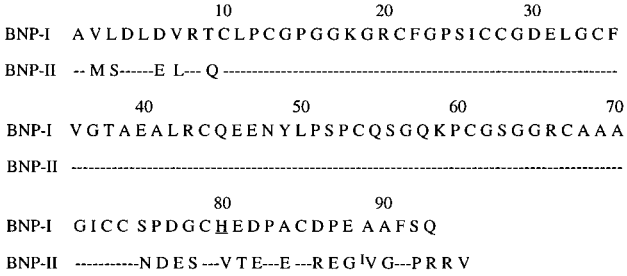

FIGURE 1: Comparison of the sequences of bovine NP-I and -II. The complete sequence of BNP-I is shown with His-80 underlined. His-80 is substituted by Glu in H80E. The sequence of BNP-II is shown where it deviates from that of BNP-I. Data are from ref *44*. Note that residue 93 of BNP-I is typically absent in the well-characterized protein derived from bovine pituitaries, and is deleted in our constructs (*8*).

Four crystal structures for BNP have been reported, that of des 1-6 BNP-II in the unliganded state and complexed with vasopressin (*5*) and of unmodified BNP-II complexed with the peptide *p*-iodo-L-phenylalanyl-L-tyrosine amide (*6*) and with oxytocin (*7*). In all four structures, BNP-II exists as a dimer in which each subunit consists of β-sheet, turns, a single 3,10 helix, and loops, and is formally divided by disulfide-pairing and homology relationships into an amino-

[†] Supported by Grant GM-17528 from NIH.

[§] Coordinates for the ensemble of 20 structures of H80E and for the average structure can be accessed from the Protein Data Bank as files 1L5C and 1L5D, respectively. NMR chemical shift data have been submitted to the BioMagResBank as entry 5565.

* To whom correspondence should be addressed. Phone: 212-746-6428. Fax: 212-746-8875. E-mail: ebreslow@mail.med.cornell.edu.

[‡] Present address: Target Structure-Based Drug Discovery Group, National Cancer Institute, Frederick, MD 21702.

[1] Abbreviations: NP, neurophysin; BNP, bovine neurophysin; BNP-I, bovine oxytocin-related NP; BNP-II, bovine vasopressin-related NP; H80E, the H80E mutant of BNP-I (previously termed the EE mutant); DES, des 1−6 BNP-II; NMR, nuclear magnetic resonance; 2D, two-dimensional; 3D, three-dimensional; NOE, nuclear Overhauser effect; NOESY, NOE spectroscopy; TOCSY, total correlation spectroscopy; HSQC, heteronuclear single-quantum coherence; FID, free induction decay; rmsd, root-mean-square deviation.

10.1021/bi012067k CCC: $22.00
Published on Web 04/11/2002

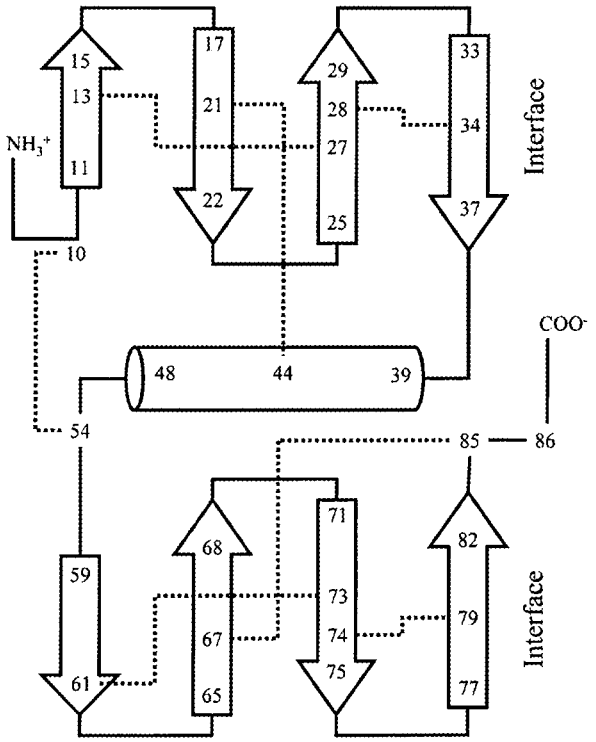

FIGURE 2: Secondary structure and disulfide pairing (dotted lines) of unliganded DES. Secondary structure assignments are based on the X-ray structure (*5*) using Swiss Protein Data Bank algorithms (*45*) and deviate subtly from the assignments used for the oxytocin complex of BNP-II (*7*) in turn vs sheet assignments, the differences reflecting the modeling program used.

domain (residues 1−54) and a carboxyl domain (residues 55−92) (Figure 2). Significantly, the binding site and subunit interface are on opposite ends of each subunit (*5*−*7*), indicating that the positive linkage between binding and dimerization is mediated by long-range communication through the protein structure. Available evidence suggests that the principal mechanism underlying this linkage involves dimerization-induced conformational changes that facilitate binding (*5*), but a more complete mechanistic understanding has been hindered by the absence of a structure for the unliganded monomeric state. Several BNP residues affected by dimerization have been identified in earlier NMR investigations (vide infra). These studies principally involved BNP-I rather than BNP-II because of the greater solubility of BNP-I complexes and the better resolution of its NMR spectra. However, the degeneracy of the proton signals in NMR spectra due to the equilibrium between monomer and dimer under normal NMR conditions, and the high degree of proton signal overlap, prevented structure determination of the unliganded monomeric state.

We recently overcame these problems by mutation of the subunit interface of BNP-I to generate mutants having reduced dimerization constants, but retaining the positive link between binding and dimerization (*8*). The dimerization constant of one of these mutants, H80E, is one-tenth that of BNP-I under similar conditions, and, at pH 7.5, is sufficiently low to allow investigation of the solution structure of the unliganded monomer. We were also able to prepare isotopically labeled samples of H80E in yields sufficient for heteronuclear three-dimensional NMR experiments and removal of the proton degeneracy. In this paper, we report studies of the solution structure of H80E that shed light on the conformational differences between unliganded monomeric and unliganded dimeric states of BNP. These differences were derived from comparison of the H80E structure with the X-ray structure of unliganded des 1−6 BNP-II (DES).

MATERIALS AND METHODS

Preparation of H80E. The expression and purification of unlabeled H80E has been described earlier (*8*). H80E was overexpressed in *Escherichia coli* strain BL21 (DE)pLys-S cells using the T7 expression system as a fusion protein in which the protein sequence is preceded by a His tag and the TrpLe leader sequence. Uniformly labeled ^{15}N- and ^{15}N/^{13}C-H80E were prepared using different protocols. ^{15}N-H80E was obtained by growing the cells at 37 °C in 1 L of M9 minimal media supplemented with unlabeled glucose (4 g/L), ^{15}N-ammonium chloride (1 g/L), kanamycin, and chloramphenicol (35 μg/mL each) and Basal Vitamin Eagle media (10 mL/L, GibcoBrl, Grand Island, NY). At an OD_{600} of 0.6−0.7, the cells were induced with IPTG (final concentration 0.5 mM), harvested by centrifugation 5 h after induction, and frozen at −80 °C until further use. Uniformly ^{15}N/^{13}C-labeled H80E was prepared using a general procedure described in Marley et al. (*9*). The cells were grown at 37 °C in 1 L of LB to OD_{600} of 0.6−0.8 and pelleted by centrifugation at 4 °C. The cell pellets were resuspended in 250 mL of ^{15}N/^{13}C-enriched M9 minimal media (^{15}N-ammonium chloride (1 g/L) and ^{13}C-glucose (1 g/L)) supplemented with kanamycin and chloramphenicol (35 μg/mL each) and Basal Vitamin Eagle media (10 mL/L). The attendant 4× increase in cell density in the transfer was found to be optimal for protein expression. The cells were then incubated at 37 °C to allow for the recovery of growth and the clearance of unlabeled metabolites. One hour after transfer of the cells from LB to M9 media, the cells were induced with IPTG (final concentration 0.5 mM) and harvested 5 h after induction. The cell pellets were frozen at −80 °C until use. The isolation of the inclusion bodies, purification of the fusion protein, cleavage of the H80E protein segment by CNBr, purification, and folding of H80E were performed as previously described (*8*). The final yields of purified ^{15}N-labeled and ^{15}N/^{13}C-labeled H80E were 1 and 2 mg/L, respectively.

Preparation of ^{15}N-Labeled Des 1−5 H80E. Site-specific cleavage of residues 1−5 in H80E was achieved by incubating 2.5 mg of ^{15}N-labeled H80E and 2 μg of Endoproteinase Asp-N in 0.5 mL of 25 mM NaH_2PO_4, pH 7.9, at 37 °C for 4.5 h. The digestion was quenched by the addition of equivolume 0.5 M EDTA, and the des 1−5 product was purified by gel-filtration. The purity and structure of the product were confirmed by electrophoresis and mass spectrometry.

NMR Spectroscopy and Data Processing. NMR samples consisted of uniformly labeled ^{15}N-H80E or ^{15}N/^{13}C-H80E dissolved in 300 μL 10% D_2O/90% H_2O to a final concentration of 1.4 mM; the pH was adjusted to 7.5 (uncorrected for isotope effects), unless otherwise noted. All experiments were run in Shigemi tubes, and the data were collected on a Varian Inova 600 MHz spectrometer equipped with a 5-mm ^{13}C/^{15}N/^{1}H triple resonance probe and pulsed field gradients. Experiments were performed at 10, 25, and 30 °C to resolve

assignment ambiguities and provide additional constraints. In 2D [^{1}H-^{15}N] HSQC and all 3D experiments, except for the simultaneous 3D ^{13}C/^{15}N-edited NOESY−HSQC experiments which used the STATES-TPPI method (*10*), quadrature detection in the indirectly detected dimension was obtained using the gradient sensitivity enhanced method (*11*). The transmitter frequencies were set to H_2O. Proton chemical shifts were referenced to the chemical shift of H_2O, which was calibrated for each temperature. ^{15}N and ^{13}C chemical shifts were indirectly referenced (*12*).

The data sets were processed using the NMRPipe software package (*13*) and analyzed using NMRView 4.1 (*14*) running on a Silicon Graphics R10000 workstation. The FIDs were processed using a solvent filter and linear prediction of the indirectly detected dimensions. A sine-bell window function was applied to each FID prior to being zero-filled, Fourier transformed, and phase corrected.

Two-dimensional [^{1}H-^{15}N] HSQC spectra (*15*) collected for ^{15}N- and ^{15}N/^{13}C-labeled H80E were used to initially assign H^N and N resonances and assess sample stability during and after the NMR experiments. HSQC spectra at 30 °C provided the best dispersion in both the ^{1}H and N dimensions, but additional ^{1}H and N resonances were detected and assigned at 10 °C. HSQC spectra were collected with sweep width and complex data points of 8000.0 Hz and 512 for ^{1}H(F_1) and 1600.0 Hz and 128 for ^{15}N(F_2).

Three-dimensional heteronuclear triple resonance experiments, HNCA (*16*), HN(CO)CA (*17*), HNCACB (*18*), CBCA(CO)NH (*19*), and HNCO (*16*) were used to correlate resonances from backbone H^N, ^{15}N, HA, ^{13}CA, and ^{13}CO and side chain ^{13}CB. All five triple resonance experiments were acquired at 30 °C. Additional HNCA and HNCO experiments were recorded at 10 °C to identify resonances absent or overlapped in the 30 °C data set and to verify assignments. For assignment of side chain aliphatic ^{13}C and ^{1}H resonances, the 3D ^{15}N-edited TOCSY−HSQC experiment (*20*) was recorded at 25 °C on the ^{15}N-H80E sample and the 3D ^{13}C-edited HCCH-TOCSY (*21*) at 30 °C on the ^{13}C/^{15}N-labeled H80E. The 3D ^{15}N TOCSY−HSQC experiment was collected with a mixing time of 61 ms with sweep widths and complex data points of 6499.8 Hz and 72 for ^{1}H (F_1), 1700.0 Hz and 48 for ^{15}N (F_2), and 8000.0 Hz and 512 for ^{1}H (F_3). For the HCCH-TOCSY experiment, the mixing period was 12 ms and the sweep widths and complex data points were 6000.0 Hz and 64 for ^{1}H (F_1), 9650.1 Hz and 64 for ^{13}C (F_2), and 8000.0 Hz and 512 for ^{1}H (F_3).

Distance and Geometrical Restraints. To obtain distance restraints for structure calculations, 3D ^{15}N-edited NOESY−HSQC were acquired at 10 and 25 °C for the ^{15}N-labeled H80E sample with a mixing time of 150 ms for both experiments. The sweep width and complex data points were 6500.0 Hz and 64 for ^{1}H (F_1), 1700.0 Hz and 40 for ^{15}N (F_2) at 10 °C, and 48 for ^{15}N (F_2) at 25 °C, and 6499.8 Hz and 416 for ^{1}H (F_3). In addition, simultaneous 3D ^{13}C/^{15}N-edited NOESY−HSQC spectra were collected on the ^{15}N/^{13}C-labeled H80E sample at 10 and 30 °C. The experiment at both temperatures used the same parameters (a 150 ms mixing period, sweep widths of 5999.7 Hz (F_1), 4070.0 Hz (F_2), and 8000.0 Hz (F_3), and complex data points of 128 (F_1), 48 (F_2), and 512 (F_3)).

The NOE cross-peaks were manually assigned using NMRView. Cross-peaks were categorized as strong (1.8−2.7 Å), medium (1.8−3.3 Å), or weak (1.8−5.0 Å) based on peak volume, with calibration from the volumes of intraresidue cross-peaks and those corresponding to known distances in derived secondary structure elements. The NOE cross-peaks in the ^{15}N- and ^{13}C-edited spectra were assigned independently, and the assignments from the different spectra were merged. Methyl and aromatic ring protons were assigned as pseudo-atoms, and a 0.5 Å correction was added to the upper bound of the distance restraint. A total of 812 NOE cross-peaks were unambiguously assigned from the ^{15}N- and ^{13}C-edited NOESY spectra.

To obtain ϕ angle restraints, J_{HNHA} coupling constants were measured from 3D HNHA spectra (*22*). The HNHA spectra were collected at 10 and 30 °C and provided 46 J_{HNHA} coupling constants, including coupling constants for glycine. The backbone ϕ angles were constrained to $-60° \pm 30°$ for $J_{HNHA} < 5.5$ Hz, $-120° \pm 60°$ for $J_{HNHA} > 7$ Hz, $-120° \pm 50°$ for $J_{HNHA} > 8$ Hz, $-120° \pm 40°$, and $-100° \pm 80°$ for $5.5 < J_{HNHA} < 7$ Hz (*23*). Additional ϕ and ψ angle restraints were obtained using the TALOS (*24*) program, which derives ϕ and ψ angle restraints based on CA, CB, HA, CO, and N chemical shifts. A total of 72 ϕ and ψ restraints were used in the structure calculations. Forty-four restraints (22 ϕ and 22 ψ restraints) were derived from TALOS, and 28 additional ϕ angle restraints were derived from the HNHA experiments.

Fifty hydrogen bond restraints were also included in the structure calculations, 14 hydrogen bonds in the helix and 36 in antiparallel β-sheets. Hydrogen bonds were derived from elements of secondary structure, the latter identified in H80E by analysis of the ΔCA, ΔCB, ΔCO, ΔHA, and $(\Delta CA - \Delta CB)_i$ chemical shift indexes, J_{HNHA} coupling constants, and medium range and a few long-range NOEs (Results). Each hydrogen bond was specified as two distance restraints (H_N−O distance of 1.3−2.5 Å and N−O distance 2.3−3.5 Å).

Structure Calculations. Structure calculations were performed on a Silicon Graphics R10000 using the simulated annealing protocol within the CNS (Crystallography & NMR Systems) 0.9 (*25*) software. Covalent structure plus the NOE, dihedral angle, and hydrogen bond constraints were used as inputs. Since individual methylene protons on a given carbon were arbitrarily assigned, the NOE restraints were treated as sum-averaged distances (*26*). Additionally, since short-range structural information can be derived from three-bond coupling constants, ^{13}C chemical shifts and ^{1}H chemical shifts, 46 J_{HNHA} coupling constants (*27*), 157 CA/CB chemical shifts (*28*) and 108 HA/H^{methyl} chemical shifts (*29*) were included as inputs in the anneal module of CNS. The calculation parameters for the input restraints were derived from Qin et al. (*30*).

In the final structure calculation, two hundred structures were generated as follows. The simulations were initially performed in torsion angle space, starting from the extended conformation of H80E, in which the native disulfide pairings were defined in the structure file. The extended conformation of H80E was heated to 50 000° K in 1000 steps with a time step of 0.015 ps and NOE and dihedral force constants of 150 and 100 kcal/mol·deg, respectively. The first slow-cool annealing stage involved a quenching to 0° K for 1000 steps with a time step of 0.015 ps and NOE and dihedral force constants of 150 and 200 kcal/mol·deg, respectively. A second slow-cool annealing was then carried out in Cartesian

space with the system temperature decreased from 2000 to 0° K in 3000 steps with a time step of 0.005 ps and a temperature step of 25° K. The NOE and dihedral force constants were 150 and 200 kcal/mol·deg, respectively. The structures were refined using 200 steps of restrained energy minimization with NOE and dihedral force constants of 75 and 400 kcal/mol·deg, respectively. The best 20 structures were selected based on their low total CNS energies and an average structure was calculated using the accept.inp module in CNS. The quality of the structures was assessed using Procheck-NMR (*31*) and MOLMOL (*32*) programs.

RESULTS

Dimerization Constants. The dimerization constants of NP and its mutants can be determined by monitoring the relative intensities of the signals at ~6.2 and 6.4 ppm in one-dimensional spectra (e.g., ref *8*); these signals have been assigned to the same proton in the monomer and dimer, respectively (e.g., ref *33*). We previously reported dimerization constants of the H80E mutant at 25 °C in 90% H_2O/10% D_2O at pH 6.1 and pH 7.5 as 2000 and <100 M^{-1}, respectively (*8*). In the present studies, we additionally obtained dimerization constants at 30 °C and pH 6.01 in 90% H_2O/10% D_2O of 1000 M^{-1} and at pH 5.5 in D_2O of 3000 M^{-1}. All the NMR experiments described in this paper were collected on samples of H80E at pH 7.5 unless otherwise noted; contributions from dimer were negligible at this pH (see also below).

Resonance Assignments. Almost all of the H80E backbone ^1H, ^{13}C, and ^{15}N resonances were assigned. Figure 3 shows the HSQC spectrum of H80E at 30 °C, with the assignments obtained at this temperature. This spectrum has the 16 expected -NH resonances from the Gln and Asn side chains, but a greater than expected number of resonances representing backbone amides. This reflects the presence of two NH resonances each for residues 3, 9, 13, 14, 21, 22, 25−28, 36, 38, 42, 44, 45, 59, 68, 69, 74, and 75. (Residues 7, 8, 41, 66, 70, 71, and 77 also appear to exhibit two -NH signals, but in these cases, definitive assignment of the second signal could not be made.) Resonances for residues 2, 10, 31, 39, 43, 64, and 86 were not seen at 30 °C. HSQC experiments at 10 °C verified the assignments made at 30 °C and led to the appearance of backbone NH resonances for residues 10, 31, 64, and 86 (see indicated positions in Figure 3), suggesting that these H^N are in rapid solvent exchange at 30 °C; Cys-10 and Arg-86 are part of unstructured loops, while Glu-31 and Gly-64 are elements of β-turns (see below). Although absent in the HSQC spectra at 10 and 30 °C, presumably due to extremely fast exchange with H_2O or line-broadening effects resulting from conformational exchange, the H^N resonances of Ala-39 and Arg-43 were traced in the ^{15}N-edited and ^{13}C-edited NOESYHSQC spectra at 10 °C. A complete assignment of the C^α resonances was obtained. From the HNCO spectra at 10 and 30 °C, 78 CO resonances were identified. The undetected CO resonances were for residues 1, 9, 11, 14, 23, 38, 42, 50, 52, 59, 75, 82, and 86.

All HA resonances except for those of Cys-10, Pro-15, and Pro-53 were identified. Among the most notable of the HA signals is that near 6.2 ppm, which characterizes the monomeric state of unliganded NP. The ~6.2 ppm signal was previously (*33*) attributed to a downfield-shifted HA proton of either Cys-28 or Cys-34; in this study, the ~6.2 ppm peak was definitely assigned to the HA of Cys-28. The presence of a signal near 6.2 ppm and the absence of the corresponding dimer signal at 6.4 ppm in all the 3D NMR experiments confirm the monomeric state of H80E during the NMR experiment. Approximately 70% of side chain ^{13}C and proton signals were assigned.

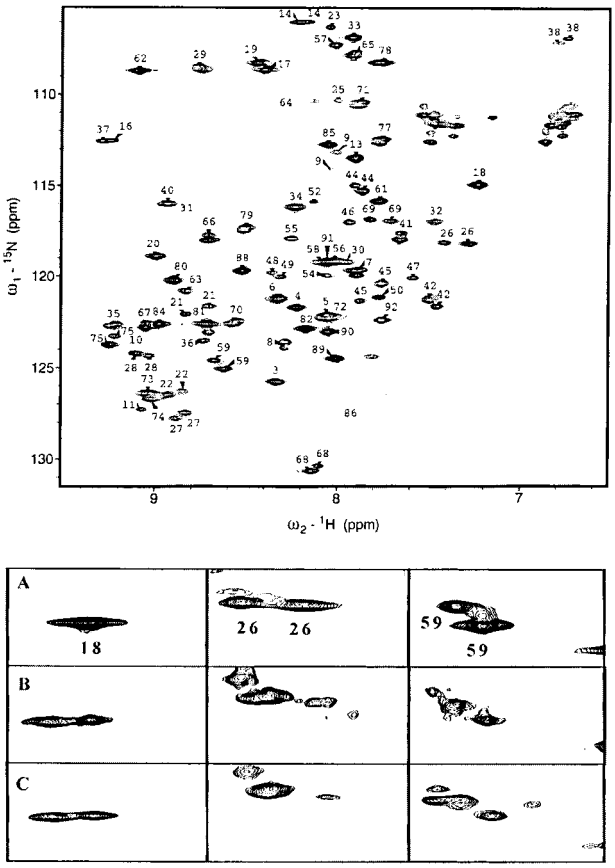

FIGURE 3: Top: -NH HSQC spectrum of H80E at pH 7.5 and 303° K, with assignments for backbone -NH signals by residue number. Signals for residues 10, 31, 64, and 86 are not seen under these conditions, but are seen at lower temperature at this pH at the positions indicated by residue number in the spectrum. Note the double signals for many residues; double signals for residues 3 and 13, reported in Results, are present but not obvious in the spectrum shown. Below: Effects of diminishing pH on the -NH HSQC signals from Lys-18, Ile-26, and Lys-59 at 298° K. A, pH.7.5; B, pH 6.0; C, pH 5.5. Note the appearance of a second component for the Lys-18 signal and the change in the relative intensities of the two main components of the Ile-26 and Lys-59 signals as the pH is lowered below 7.5. (The signal that appears in the upper left of the Ile-26 box at pH 6 and 7.5 and the signal furthest to the right in the pH 5.5 Lys-59 box are unassigned.)

Proton resonance assignments for H80E residues at the N- and C-termini are in good agreement with those determined for the BNP-I dimer in previous 1D and 2D $^1H-^1H$ NMR experiments (e.g., Table 1). Since the amino and carboxyl loops are unstructured, their proton chemical shifts in both H80E and BNP-I are near random coil values. However, (Table 1), differences between the BNP-I dimer and the H80E monomer were detected for several residues that had assigned signals (*34*) in the BNP-I dimer. At pH 6.2, the chemical shift of the methyl protons of Ala-68 is 0.37 ppm in the unliganded BNP-I dimer and 0.69 ppm in H80E. The >0.3 ppm downfield shift of the Ala-68 H^β resonance in H80E relative to the BNP-I dimer is consistent with earlier observations that the 0.37 ppm BNP-I dimer

Table 1: Comparison of Selected ^{1}H Chemical Shifts in H80E and BNP-I[a]

atom	BNP-I (ppm)	H80E (ppm)	random coil (ppm)
Val 2, −7 H^{α}	4.15	4.12, 4.13	4.18
Val 2, −7 H^{β}	2.15	2.04, 2.11	2.13
Val 2, −7 H^{γ}	0.9−1.0	0.94, 0.90	0.97, 0.94
Leu 3, −5 H^{α}	4.2−4.5	4.36, 4.26	4.38
Leu 3, −5 H^{β}	1.63	1.58	1.65
Leu 3, −5 H^{γ}	1.63	1.58	1.64
Leu 3, −5 H^{δ}	0.9−1.0	0.87, 0.86	0.94, 0.90
Thr 38 H^{α}	5.00	4.54	4.35
Thr 38 H^{β}	4.51	4.71	4.22
Thr 38 H^{γ}	0.40	1.27	1.23
Ala 68 H^{α}	3.95	3.97	4.35
Ala 68 H^{β}	0.37	0.69	1.39
Ala 89 H^{β}	1.38	1.34	1.39
Ala 90 H^{β}	1.28	1.26	1.39
Phe 91 H^{β}	3.05	3.20/3.02	3.22/2.99
Ser 92 H^{α}	4.29	4.22	4.50
Ser 92 H^{β}	3.85	3.81	3.88/3.88

[a] Assignments for BNP-I for residues 2, 3, 5, 7, and 89−92 are from ref *43*; other assignments are from ref *34*.

signal must shift downfield by at least 0.26 ppm in the monomer (*34*, *35*). Structural changes potentially contributing to the changes in Cys-28 and Ala-68 chemical shifts are given in the discussion. Similarly, the chemical shift of Thr-38 methyl protons in H80E is 1.27 ppm, as opposed to 0.4 ppm in dimeric BNP-I (Table 1), again consistent with the loss of signal at 0.4 ppm (*35*) accompanying dimer dissociation. In this case, the upfield shift in the dimer is due to strong shielding by Phe-35 of the adjacent subunit.

Secondary Structure Elements. The chemical shift index, J_{HNHA} coupling constants, ϕ and ψ dihedral angle constraints from TALOS, and NOE assignments were used to identify secondary structure elements in H80E, as described by the following.

Relative to random coil chemical shifts, CA and CO resonances tend to shift downfield in helices, while CB and HA resonances tend to shift upfield; the opposite holds true for β-sheet and extended structures (*36*). In the case of H80E, the deviations (Δ) of these resonances from random coil values gave only short stretches of all-positive and all-negative values (data not shown), potentially reflecting chemical shift perturbations by aromatic rings and probably also the unusually high disulfide content (Figures 1 and 2). Analysis of the chemical shifts of protons <5 Å away from disulfide bonds shows that most are shifted upfield relative to their value in unstructured peptides. To address this, the difference between ΔCA and ΔCB was calculated using a three-point smoothing function: $(\Delta CA - \Delta CB)_i = (\Delta CA_{i-1} + \Delta CA_i + \Delta CA_{i+1} - \Delta CB_{i-1} - \Delta CB_i - \Delta CB_{i+1})/3$, as described elsewhere (*37*). Consecutive positive and negative $(\Delta CA - \Delta CB)_i$ values identify helical and sheet regions, respectively. Figure 4 shows the $(\Delta CA - \Delta CB)_i$ plot for H80E and the secondary structure for different regions indicated by the data. Helical structure is indicated for residues 38−48 and 84−89, while residues 9−14, 19−21, 25−28, 33−37, 59−62, 67−69, 72−75, and 78−83 are assigned by the data as β-strands.

Most of the J_{HNHA} coupling constants and ϕ and ψ dihedral angle constraints were consistent with the $(\Delta CA - \Delta CB)_i$ secondary structure analysis. The main discrepancy was in the helix. J_{HNHA} coupling constants, obtainable only for residues 41, 44, and 46, were higher than typically associated

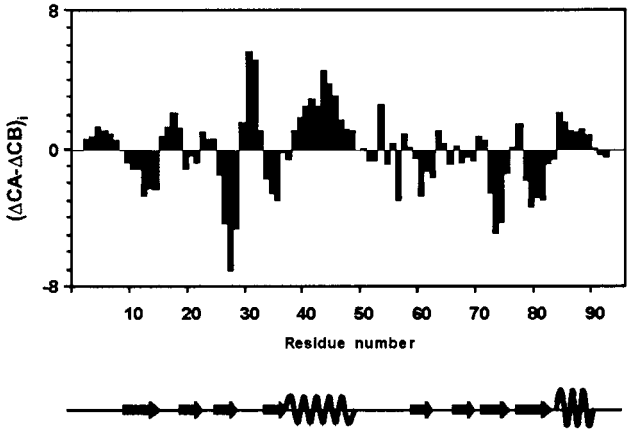

FIGURE 4: Plot of $\Delta CA - \Delta CB$ for H80E. Secondary structure assignments based on the data are shown below. Data were calculated and analyzed as in ref *37*.

with helical structure. However, self-consistent TALOS-predicted ϕ and ψ values for residues 39−40, 42−43, and 45 fell within the helix regions of the Ramachandran plot.

NOE data (Figure 5) also accord with the $\Delta CA - \Delta CB$ analysis. Clusters of NOEs normal to the diagonal represent residues within β-strands, with strand pairing indicated by the position of the NOE cluster. Two 4-stranded β-sheets in H80E are identified by these criteria within the sequences 12−36 and 59−81, although the NOE density is lower than predicted by the structure of unliganded DES (Figure 5). Clusters of NOEs along the diagonal represent a high number of short-range NOEs ($i - j \leq 4$) and typically describe helical structures. The relatively high NOE cluster density along the diagonal for residues 40−47 suggests helix, but is again lower than that calculated from the DES structure (Figure 5), and the particularly marked deficiency of NOEs relative to DES for residues 48−50 suggests that this region deviates significantly in structure from DES. A high NOE density along the diagonal for residues 82−88 also indicates a short coiled or helical segment near the protein's C-terminus. Figure 5 also demonstrates, that, although the number of interresidue NOEs in H80E is fewer than in DES, the residues involved in interresidue NOEs in H80E are the same as those in DES, with the exception of an ambiguous NOE to residue 57 in H80E from either residue 22, 52, or 59, none of which are predicted by the DES structure. However, the identities of the specific contacts between some residues can also be shown to differ in H80E from those predicted by the DES structure.

In sum, the data indicate helical structure for residues ~39−~48, sheet structure for the approximate regions 11−37 and 59−83, unstructured loops for residues 1−10 and 49−58, and the presence of coil within 82−92. The results indicate that H80E and DES possess largely similar secondary structures. These similarities are confirmed and extended by the calculations below.

Structure Calculations and Quality. Inputs for the structure calculations include 811 unambiguous NOE distance restraints (392 intraresidue, 292 medium range, and 127 long range), 50 hydrogen bond distance restraints, 72 torsion angle constraints (50 ϕ and 22 ψ torsion angle restraints), 46 J_{NHA} coupling constants, 157 CA/CB and 108 ^{1}H chemical shift restraints and the pairing of the protein's seven disulfides. The NOE to Gly-57 was treated as ambiguous (*25*), with

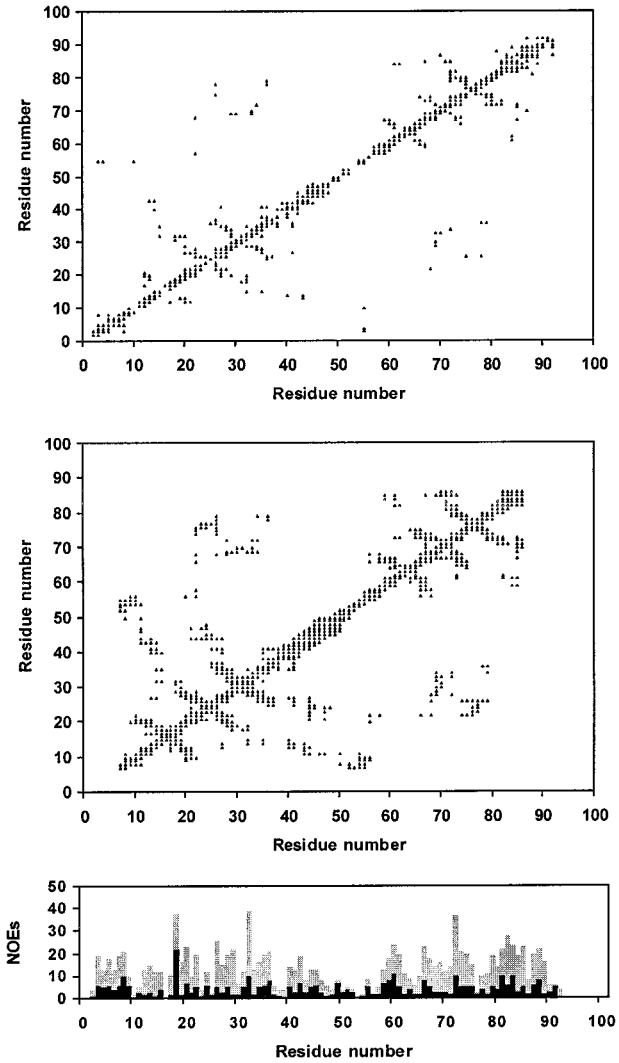

FIGURE 5: Demonstrated proton−proton NOEs for H80E (top) compared to that *predicted* for DES from its structure (center). Predicted DES NOEs do not include those involving side chain -NH groups, since these were not examined in H80E. Data for H80E omit the ambiguous NOE to Gly-57 (text). Bottom chart shows the number of observed NOEs/residue in H80E. Intraresidue NOEs are shown in black, and interresidue NOEs are shown in gray.

the three possibilities as given above. The final 20 structures and an average structure were generated using the protocol described in Materials and Methods. The quality of the 20 structures was assessed using Procheck-NMR; 91.9% of ϕ and ψ angles fall within the most favorable or allowable regions, 7.4% in the generously allowable region and 0.7% in the disallowed region. Many of the residues in the generously allowed and disallowed regions are from the unstructured (loop) regions of H80E. Figure 5 shows the number of NOEs per residue. For residues within the helix and sheets (including turns), the average number of NOEs per residue is 14.8, suggesting that the structured regions are relatively well defined by NOE restraints. The presence of 14 glycine and 9 alanine residues in H80E limit the number of possible side chain NOEs. Among the three unstructured regions of H80E, the middle loop is the most poorly defined as indicated by its average NOE value of 4.0. No NOE restraints were assigned to Pro-53 and two each to Cys-54 and Ser-56. In addition to the treatment of the NOE to Gly-57 as ambiguous, we separately calculated structures

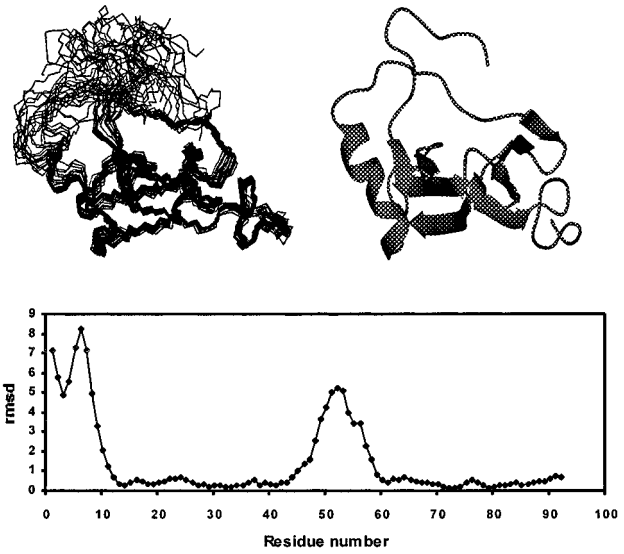

FIGURE 6: Calculated backbone structure of H80E. Top left: superimposition of the 20 lowest energy structures. Top right: calculated average structure shown in ribbon format. In both structures, the amino terminus is at the upper right, and the carboxyl terminus is at the lower right. The chart shows the calculated rmsd of the 20 structures from the mean.

for each of the individual possibilities, as well as a structure deleting this NOE together. The calculated structures differed from each other in loop conformation and in their prediction of a subset of specific intramolecular contacts, but were of similar energies and otherwise of similar conformation. Unless otherwise noted, all of the discussion and conclusions below pertain only to those features of the structure that are independent of the NOE assignment to Gly-57.

Calculated Structure(s). The average calculated NMR structure begins with a loop (residues 1−10), followed by a four-stranded β-sheet (residues 11−15, 17−21, 25−29, 33−37), an ambiguous three-turn 3_{10} helix (residues 39−48, according to MolMol [32]), a long loop (residues 50−58), another four-stranded β-sheet (residues 59−61, 65−68, 71−75, 78−82) and a long C-terminal partially coiled loop (residues 83−92). Classification of the 39−48 region as strictly helical is dependent on the modeling program used, indicating that the helix is less perfect than in DES. Nonetheless, the results are consistent with the initial secondary structure analyses (vide supra) and indicate similar secondary structures for the H80E monomer and DES dimer (cf. Figure 2). This accords with earlier studies demonstrating a lack of effect of dimerization on the far UV circular dichroism spectrum of NP (*38*), supporting the validity of the general structure.

The 20 NMR structures were superimposed by minimizing the rmsd of the backbone atoms of residues 11−45 and 59−82 relative to the mean structure (Figure 6) The rmsd of the 20 structures about the mean coordinate position is 1.47 Å for backbone atoms, 1.71 Å for all atoms and 0.58 Å for backbone atoms in the structured regions of the protein. Sheet and helix elements are well ordered except for residues 45−48 of the helix (Figure 6), which have a backbone rmsd >1 Å. In contrast, the backbone rmsd for helix residues 39−44 is 0.47 Å and that for the β-sheets in the amino and carboxyl domains is 0.39 and 0.41 Å, respectively.

The regions of H80E showing the least structural organization are the amino loop (residues 1−10) and the middle

loop (residues 50−58) (Figure 6). The high backbone rmsd values for these loops and for the C-terminus of the helix (vide supra) are in part the result of two potential orientations of the amino loop relative to the region representing the end of the helix and the middle loop. The amino loop is "threaded" through the binding site in 4 of the 20 structures and "adjacent" to the binding site in 16 structures (not shown). The tethering of the amino loop to the middle loop is demonstrated by three NOEs between them: HA of residues 3 and 4 to H^N of residue 55 and H^N of residue 10 to H^β of residue 55, but the dearth of other NOEs allows the two different potential conformations of the amino loop. The distance between the CA of Glu-47 and the CA of Pro-53 is 6.6 Å in the "adjacent" structures and 12.3 Å in the "threaded" structures, the larger value allowing the middle loop to accommodate the amino loop. Several binding site residues are in this region (e.g., residues 47, 48, 50, 52, 54), the results therefore suggesting that the amino loop partially blocks the binding site in unliganded H80E (Discussion).

The structure of the NP carboxyl terminus has not been previously determined either in solution or the crystal. The solution structure of H80E showed that the 83−92 region is a twisted coil with several bends, consistent with its positive $(\Delta CA - \Delta CB)_i$ deviation (Figure 4) and the high number of NOE contacts along the diagonal (Figure 5). Compared to the amino and middle loops, the carboxyl loop displays much less disorder, with rmsd values among structures comparable to those in the β-sheet region (Figure 6).

Conformational Heterogeneity. As described above, over 25% of H80E residues exhibit two NH signals in HSQC spectra (Figure 3). These residues represent essentially all regions of the protein, and we have found no structural basis with which to correlate their distribution. The doubling is principally apparent in -NH HSQC spectra, but double signals have also been observed for CB of Cys-21 and Ala-68, which show double -NH signals, and for CB of Leu-50, which does not show a double -NH signal. We have found no obvious differences in the identity of TOCSY or NOESY connectivities of the two components of the different doublets, but differences in the intensity of NOE connectivities were occasionally observed (the more intense NOE used for the structure calculation).

The HSQC pattern is independent of protein preparation, and evidence of exchange between the two components of the doublets can unambiguously be seen with several residues under the right conditions; e.g., residues 42 and 59 at 30 °C and residue 26 at 25 °C in Figure 3. The results indicate that the calculated structure is an average of at least two slowly exchanging conformers, with an estimated exchange rate <10/s based on the 150 ms mixing time of the experiments. This is a very slow rate. Very slowly exchanging conformers of Tyr-49, suggestive of hindered ring rotation, were previously observed in the unliganded dimeric state of BNP-I, but were not seen in the BNP-I monomer (*38*) and do not appear to be present in monomeric H80E. Cleavage of the first five residues of H80E by treatment with Asp-N did not alter the double nature of the remaining observable -NH signals, although it led to the loss of signals from residues in the 6−9 region and within and adjacent to the loop (e.g., residues 48, 52, 54, 55), presumably by increased rates of solvent exchange. Thus, the conformers represented by the "doublets" are independent of interactions between the loop and amino terminus. The possibility of cis−trans Pro isomerization is not excluded. However, no cis-Pro residues are evident in crystal structures of BNP-II dimers or in the derived H80E structure, and only half of the double -NH signals are within 5 Å of a Pro residue in H80E.

Comparison of NMR and X-ray Structures. To probe structural differences between unliganded monomeric and dimeric states, the NMR structure of H80E was compared with the X-ray structure of unliganded DES. The two subunits of the DES dimer are almost identical, with a rmsd of backbone atoms relative to the mean of 0.08 Å; subunit A was selected for comparison to H80E. The shortened amino acid sequence of DES, and the fact that DES residues 87−95 are not located in the crystal structure (*5*), allow structural comparison to H80E only for residues 7−86. Among these 80 residues, 11 are not conserved between H80E and DES, two in the amino domain and nine in the carboxyl domain (Figure 1).

The average NMR structures of H80E was superimposed on that of DES so as to obtain the best fit of all backbone atoms ("all-fit" comparison), or to minimize the backbone rmsd for residues 11−45 and 59−82 ("best fit" comparison). The rmsd values for the backbone atoms for both types of fit are plotted in Figure 7. The regions differing between the two proteins are seen to be independent of the type of fit chosen, although rmsd values, particularly for the helix and 50−58 loop, quantitatively differ for the two types of fit. Because the loop is the most poorly defined part of the structure, the "best-fit" comparison is probably the comparison of choice.

Comparison of the two structures indicates the largest rmsd values for the amino loop (residues 7−10), the carboxyl half of the helix (residues 45−48), most of the middle loop and the 62−64 turn, with lesser but still significant differences dispersed through other regions; differences in the helix principally reflect helix orientation (Figure 8), not the small secondary structure differences that also appear to be present (see also Discussion). It is relevant that the differences between H80E and DES in average conformation (Figure 7) are also seen when the DES structure is superimposed on the mixture of calculated H80E structures (Figure 9), even in the middle loop region, indicating that they largely fall outside the likely uncertainty of the H80E structure. Regions showing rmsd values >1 Å can be shown to include the majority of peptide binding site residues (e.g., residues 7, 8, 10, 24, 47, 48, 50, 52, 54, 76) while almost all interface residues (e.g., residues 32−38, 78−80) have lower rmsd values. Residues 62−64, which show particularly high backbone rmsd values, and residues 70 and 86, which also show rmsd values >1 Å, are not directly involved in either binding or dimerization. However, of potential significance is that residues 62−64 and 70, together with residues 17, 24, 31, and 76, which represent either rmsd values >1 Å, or local maxima in the rmsd plot, represent all the central β-turns of the protein. Factors contributing to the differences in the two structures, and the potential implications of the similarities and differences are discussed further below.

Spectral Changes Associated with Dimerization. Differences between the structures of H80E and DES contain contributions from factors additional to differences between monomeric and dimeric states (see below). To obtain a

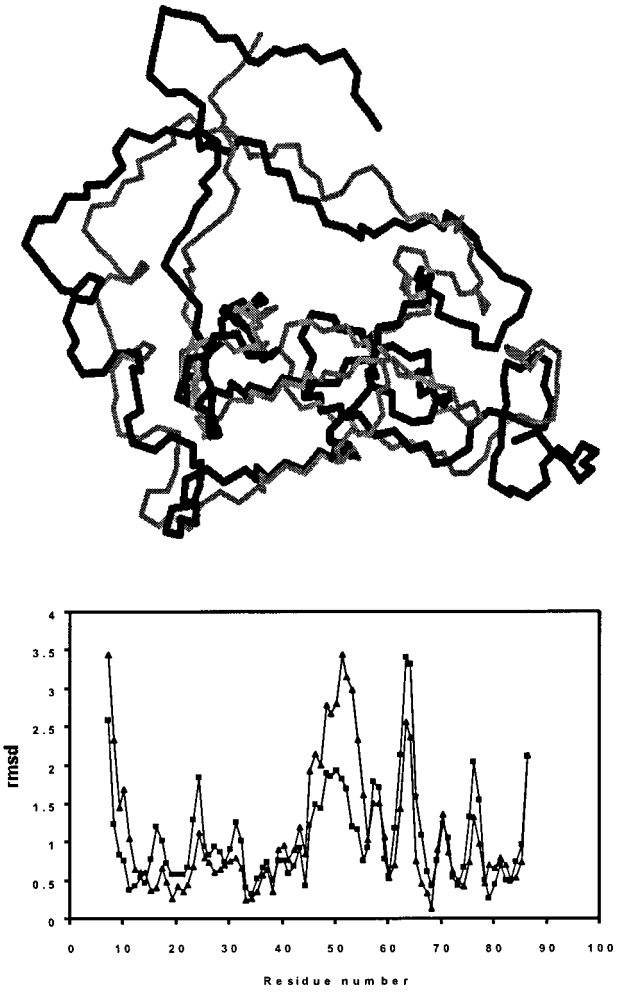

FIGURE 7: Comparison of the average backbone structure of H80E (black) with that of the crystal structure of DES (gray). Orientation is the same as in Figure 6. Rmsd values for the structural comparison are shown below, calculated on the basis of the fit of all backbone atoms ("all-fit" model, squares), or on the basis of the fit of β-sheet and helix atoms ("best-fit model", triangles), as described in the text.

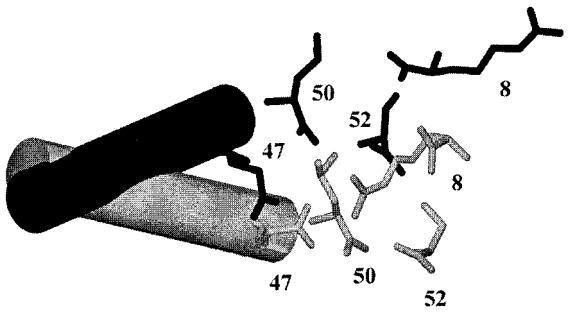

FIGURE 8: Relative orientation of the 3,10 helix in H80E (black) and DES (gray), also showing binding site residues Arg-8, Glu-47, Leu-50, and Ser-52. Note that close proximity of Glu-47 to Arg-8 in DES reflects the presence of a salt bridge between their termini and that these residues are too far apart and inappropriately oriented in H80E to form a salt bridge.

preliminary but direct view of the effects of dimerization on H80E, we compared the HSQC spectrum of the H80E monomer at pH 7.5 with spectra at pH 6.0 and 5.5 (Figure 3), the latter spectra representing 60 and 70% dimer by weight, respectively. Changes in HSQC spectra with pH over this region arise from specific effects of dimerization and/

FIGURE 9: Superimposition of the structure of DES (black) on the 20 lowest energy structures of H80E (gray). Left: Structures are in the same orientation as in Figures 6 and 7. Right: Structures are rotated 180° relative to Figures 6 and 7. Note regions exhibiting lack of masking of DES by any corresponding H80E segment.

or protonation on individual residues, the effects of changes in correlation time on all residues, and intensity changes arising from decreased rates of proton exchange with solvent. In this case, we note that there is a large intensity decrease for most residues at the lower pH, with the notable exception of residues 64 and 86, the signals of which increase in intensity due to decreased solvent exchange rates (data not shown). These intensity changes complicate analysis of the lower pH spectra. However, chemical shift changes are seen for a number of residues. Some of these are interface residues (data not shown), while others, for example, residues 18, 26, and 59 (Figure 3), are not. The Lys-18 signal develops a downfield component at the lower pH, and the two components of the Ile-26 and Lys-59 signals change significantly in relative intensity and/or chemical shift, suggesting a difference in the mix of conformers that contribute to monomeric and dimeric states in solution. Note that neither 18, 26, or 59 are sufficiently near groups indicated by NMR spectra to titrate in this region that these effects should arise from neighboring group protonation. The relevance of these changes is discussed further below.

DISCUSSION

Potential Contributions to the Structural Differences between H80E and DES: To What Extent Do the Differences Reflect Differences between Unliganded Monomeric and Dimeric States? The differences in the derived structures of the H80E BNP-I monomer and des 1−6 BNP-II dimer arise not only from intrinsic differences in monomer and dimer conformation, but potentially also reflect sequence differences between the two proteins (Figure 1), the impact of crystal packing forces on the crystal structure of DES, and some of the inherent ambiguities of NMR. This last is of particular significance when NMR is applied to systems exhibiting conformational interchange and regions of relatively low order, as is the case here—situations that have the potential respectively to generate interstructure NOEs on one hand and an insufficiency of NOEs for conformational definition on the other. Of these, the likelihood of contributions of monomer−dimer exchange to the observed NOEs, which would bias the structure toward that of the dimer, is diminished by the lack of the prominent exchange cross-peak between the monomer (6.2 ppm) and dimer (6.4 ppm) Cys-28 HA signals that characterize NOESY spectra of the unliganded BNP-I dimer (e.g., ref *34*). The potential contribution of the other factors to structural differences in individual regions is considered in the discussions below.

Structural Differences in Residues 1−20. Given the impact of cleavage of residues 1−5 from H80 (vide supra), primary structure differences, particularly the absence of residues 1−6 in DES, and possibly also differences at residues 7 and 9 (Figure 1), probably contribute significantly to the large differences between DES and H80E in the 7−10 region. However, the dimerization-induced changes in the HSQC spectrum of Lys-18 (Figure 3) suggest that dimerization contributes to the small differences in the 16−18 region (Figure 7), which includes a turn.

Structural Differences in Residues 21−31. The calculated differences between H80E and DES in the 21−31 region are particularly significant, although less pronounced than differences in some other regions on an rmsd basis. This region is reasonably well constrained with an average backbone rmsd among the best 20 structures of ∼0.5 Å, the constraints including NOEs between specific side chain atoms of Ile-26 and Pro-24 (a central binding site residue [e.g., 5]), that are not predicted from the DES structure, and which reflect tighter packing between these two side-chains in H80E than in DES. The contribution of true differences between monomer and dimer to the differences between H80E and DES in this region is evidenced in part by the dimerization-induced change in Ile-26 HSQC signal (Figure 3), the downfield signal markedly increasing at the expense of the upfield signal. Ile-26 is not at the subunit interface, but plays an important role in interdomain interactions; analysis of the differences in Ile-26 contacts between DES and H80E indicates that these include a loss in H80E of almost half of the Ile-26 interdomain packing interactions seen in DES. Thus, local interactions of Ile-26 with Pro-24 in H80E appear to be increased at the expense of interdomain interactions.

The calculated changes in this region are also consistent with the changes in Ala-68 HB resonances upon dimer dissociation (vide supra). This signal is located at 0.37 ppm in dimers of both unliganded BNP-I (*34*) and H80E (*8*), with preliminary data indicating a similar location in the unliganded BNP-II dimer (unpublished results). The large upfield shift relative to a random coil value of ∼1.4 reflects strong interdomain shielding by the face of the Phe-22 ring in the DES structure and possibly also proximity to the sulfur atoms of Cys-28 and Cys-74. In the H80E monomer, the HB signal is shifted to 0.64 ppm (vide supra) with retention of an NOE to the Phe-22 ring. The H80E structure explains the Ala-68 chemical shift change by rearrangements that move the Ala-68 methyl group from the direct center of the Phe-22 ring in DES, ∼0.7 Å closer to the ring periphery in H80E (and also 1.8 Å further from the sulfur of Cys-74). The results are significant not only because the involved region (21−28) contains several binding site residues, but also because it supports the view that that interdomain contacts remain in the monomer but in an altered state. (Note that the chemical shift of the Ala-68 methyl group in the monomer is ∼0.8 ppm upfield from the random coil chemical shift of an Ala HB so that the demonstration of an NOE between Ala-68 and Phe-22 in the monomer is unlikely to result from a chemical exchange contribution from dimer.) The difference between H80E and DES in Phe-22 to Ala-68 contacts can be shown to be paralleled by significant differences in other interdomain contacts to Phe-22, the H80E structure suggesting relatively widespread small differences between the two proteins in interdomain contacts.

The differences between the H80E and DES structures in the 21−28 region also account for the shift in the Cys-28 HA signal from 6.4 ppm in the dimer to 6.2 ppm in the monomer, which is seen in BNP-I, BNP-II, DES, and many BNP mutants (*8*, *33*, *34*). Cys-28 is not an interface residue. The downfield shift of its signal relative to the chemical shift of Cys-34 HA (5.44 ppm in H80E), its disulfide partner, is explained in DES by its simultaneous in plane proximity to the edges of both Phe-22 and Phe-35 rings of the same subunit. In the calculated H80E structure, NOEs also constrain the Cys-28 CA near the two rings, but its orientation relative to Phe-22 is altered such that it is located partially over the face of the ring, reducing the net deshielding effect on the α-proton.[2]

The Interface Region 32−38. The relatively small backbone differences between H80E and DES in this region demonstrate that this segment of the interface backbone is largely preformed in the monomer. However, the central interface residue Cys-34 also participates in intrachain interdomain interactions at <4.5 Å that differ significantly between H80E and DES, as exemplified most clearly by the dimerization-mediated changes in Ala-69 environment (see below).

Structural Differences in the Helical Region 39−49. Evidence that conformational differences between H80E and DES in this region at least in part reflect intrinsic differences between the unliganded monomeric and dimeric states is found in the dimerization-induced changes in NMR behavior of the Tyr-49 ring in both BNP-I and -II (*38*), a result initially suggesting that Tyr-49 was located at the subunit interface (*35*). Given the fact that NP dimerization is relatively independent of either cleavage of the helix after Glu-47 (*33*), or deletion of Glu-47 (*39*), dimerization-induced changes in the helix are surprising, but might potentially be mediated by contacts between residues at the N-terminus of the helix and either interface residues 35−36 or the dimerization-sensitive Ile-26 region (e.g., Figure 5).

Nonetheless, sequence differences between BNP-I and -II almost certainly contribute to the differences between H80E and DES in helix orientation. Unliganded BNP-I on one hand, and BNP-II and des 1−6 BNP-II on the other, differ in the interactions of Glu-47 in the unliganded state; a salt bridge between the carboxyl of Glu-47 and Arg-8 that is present in unliganded BNP-II and des 1−6 BNP-II (*5*) is significantly weaker or absent in this state in BNP-I in both the unliganded monomeric and dimeric states (*40*). (It is present in both proteins in the liganded state.) While reasons for this difference are unclear, this salt bridge is also absent in H80E (residues 8 and 47 are too far apart [Figure 8]), suggesting that this is an intrinsic characteristic of BNP-I-related NPs and supporting the calculated structure of H80E in this region.[3]

Structural Differences in the 50−58 Loop. The 50−58 loop extends from the C-terminus of the helix to the

[2] Qualitatively similar explanations of the Cys-28 HA chemical shift change to that in the text are found in the structures generated by specific assignment of the Gly-57 NOE to either residue 22 or 52, or by deletion of the NOE. However, no clear explanation is provided by the structure generated by assignment of the NOE to residue 59.

beginning of the first β-strand of the carboxyl domain, and contains an interdomain subsection (residues 55−58). The large differences in the two proteins calculated for the loop probably derive in part from the difference between the two in helix orientation (vide supra), and in part from the absence of residues 1−6 in DES. They do not derive from the ambiguous NOE to residue 57 in H80E (vide supra), since large differences persist when this NOE is deleted from the structure calculations and with structures representing the individual NOE possibilities. We have previously presented evidence indicating that the amino-terminus of BNP-II is involved in a set of intramolecular interactions that preferentially stabilize an additional monomer conformer and that probably involve the loop region (*33*). In the present study, we find NOEs between residues 3 and 4 of H80E and residue 55 of the loop, and a marked effect of cleavage of residues 1−5 on the HSQC -NH signals of residue 55 and of other loop residues (vide supra). Thus interactions between the loop and amino-terminal regions are confirmed in this study and would be expected to contribute to differences in loop conformation between H80E and DES.

However, significant NMR evidence of dimerization-generated differences in the 50−58 loop is found in the effects of dimerization on both Tyr-49 (*35*) and Lys-59 (Figure 3), the two residues bracketing the loop ends. We have additionally demonstrated that dimerization-induced NMR changes in BNP-I near 1.7 ppm (*35*) originate from one or both of the two Lys residues (*41*), and these changes, which are also seen in H80E, are now assigned to HB of Lys-59 based on the present chemical shift assignments. Finally, the effects of mutation or chemical modification of the 50−58 loop (*39*) indicate differences between monomer and dimer in preferred loop conformation. Mutation of Gly-57 to Ser, for example, decreases the dimerization constant by ~75% without an apparent decrease in monomer stability (*39*), strongly suggesting long-range linkage between dimerization and loop structure.

H80E Conformation in the Carboxyl Domain: Residues 60−92. The structure of the carboxyl domain is well constrained (e.g., Figures 5 and 6) and the large differences between H80E and DES in this region, which strikingly reflect differences in β-turns, are relatively unambiguous. Sequence differences between DES and H80E in the region 75−92 (Figure 1) are likely to be particularly influential in this region and may be responsible for the unusually large differences between the two proteins in the 62−64 turn, where residues 61 and 62 are shown by NOEs in H80E to establish different contacts to residue 84 (Glu in DES and Ala in H80E) than compatible with the crystal structure of DES. Relevant also is that temperature factors for the DES structure and differences between the two DES subunits are highest for the 62−64 β-turn, suggesting a degree of conformational flexibility for this turn that might permit crystal packing forces to be particularly important in the solid state.

Nonetheless, intrinsic monomer−dimer differences contribute to differences between H80E and DES in this region. Dimerization-dependent changes in Ala-68 environment have been discussed above and are also clearly seen for turn residue Ala-69. Previous NMR studies of the effects of dimerization on BNP-I identified a large concentration-dependent change in a proton signal centered at ~1.2 ppm in the monomer (*35*). This same dimerization-induced change (centered at 1.16 ppm) is identified by the chemical shift assignments in H80E as originating from the methyl group of Ala-69. Analysis of differences between H80E and DES in Ala-69 environment indicates large changes in its direct interactions with the N and CB of Cys-34 and the S of Cys-28.

Potential Relationship of the Data to Neurophysin Allosteric Mechanism. The estimated difference in binding affinity between a neurophysin dimer site and a monomer site is a factor of ~10 (*42*) or 1.4 kcal/mol, so that relatively small structural differences between the two states may be responsible for the binding difference. Comparison of the structures of the H80E monomer and DES dimer reveals a number of differences in all regions directly involved in hormone binding, particularly those involved in the critical interactions (e.g., 1) with the hormone α-amino group and tyrosine side chain. Pro-24 in particular is a central contact of the hormone tyrosine ring, while Glu-47 in the helix and residues 50 and 52 of the central loop are critical to binding the hormone α-amino group (e.g., 5). The calculated distances between pairs of binding site residues in unliganded DES and H80E indicates marked differences between the two proteins in interresidue separation; e.g., the distance between the CA atoms of Pro-24 and Glu-47 is ~5 Å longer in H80E than in DES.[4] To the extent that these particular changes reflect true monomer−dimer differences, they suggest a lesser degree of binding site pre-organization in the monomer than in the dimer. A potential alternative explanation—that blocking of the binding site by the amino-terminus (threaded structure) is more important in the monomer than in the dimer—appears inadequate to explain the 10-fold difference in binding affinity between monomer and dimer. While interactions between the amino-terminus and middle loop in BNP-II are stronger in the monomer than in the dimer, cleavage of residues 1−6 led to only a doubling of binding affinity under concentration conditions at which monomer was the principal reacting species (*33*).

An underlying question is the mechanism by which dimerization leads to intrachain conformational change. Relevant in this context is evidence above that differences between H80E and DES in interdomain interactions, several turns and in the 50−58 loop, half of which connects the two domains, appear in part to reflect dimerization-mediated effects, and to include residues that simultaneously participate in both interdomain and intersubunit interactions. The differences in interdomain interactions can be shown to be paralleled by differences between the two proteins in the distances between the interface regions of their two domains,

[3] The derived helix orientation in H80E, which places Arg-8 and Glu-47 too far apart to form a salt bridge, partly reflects the absence of NOEs between the helix C-terminus and the rest of the protein. This can be contrasted with NOEs predicted for the salt bridge-containing DES structure (Figure 5). The independent evidence of an extremely weak or absent salt bridge in unliganded BNP-I, the parent of H80E, suggests a different helix orientation in this protein as well, and argues that the NOE pattern of the helix in H80E is a valid indicator of distance.

[4] The difference in this distance in the two proteins is essentially independent of the specific assignment of the Gly-57 NOE, but is reduced to 3.5 Å if the NOE is assigned to residue 52.

α-carbon distances between the centers of the two interface regions averaging ~1 Å less in H80E than in DES. The contributions of sequence differences between H80E and DES (Figure 1) to these effects remain to be more accurately determined. However, the data tentatively suggest a model in which the dimerization-induced conformational change in NP arises from the participation of both the amino- and carboxyl domains in dimerization, with subtle differences in their relative orientation−achieved by changes in turns and in interdomain interactions and connections−needed to optimize monomer−monomer packing interactions. A related model, in which small dimerization-induced dislocations at either interface are propagated through the structure by their impact on interdomain interactions, is not precluded.

ACKNOWLEDGMENT

The authors are particularly grateful to Professor Clay Bracken of this department whose generous guidance and advice have been essential to this project, and to Professor David Peyton of Portland State University for valuable discussions at its inception.

SUPPORTING INFORMATION AVAILABLE

Assignment of proton and of backbone ^{15}N resonances for the H80E mutant of bovine neurophysin-I at pH 7.5 at 10, 25, and 30 °C; assignment of ^{13}C resonances at pH 7.5 at 30 °C. This material is available free of charge via the Internet at http://pubs.acs.org.

REFERENCES

1. Breslow, E., Burman, S. (1990) *Adv. Enzymol. 63*, 1−67.
2. Nicolas, P., Batelier, G., Rholam, M., and Cohen, P. (1980) *Biochemistry 19*, 3565−3573.
3. Kanmera, T., and Chaiken, I. M. (1985) *J. Biol. Chem. 4*, 8474−8482.
4. de Bree, F. M. (2000) *J. Neuroendocrinol. 12*, 589−594.
5. Wu, C. K., Bing, H., Rose, J. P., Liu, Z.-J., Nguyen, T. L., Zheng, C., Breslow, E., and Wang, B.-C. (2001) *Protein Sci. 10*, 1869−1880.
6. Chen, L., Rose, J. P., Breslow, E., Yang, D., Chang, W. R., Furey, W. F., Jr., Sax, M., and Wang, B.-C. (1991) *Proc. Natl. Acad. Sci. U.S.A. 88*, 4240−4244.
7. Rose, J. P., Wu, C. K., Hsaio, C. D., Breslow, E., and Wang, B.-C. (1996) *Nat. Struct. Biol. 3*, 163−169.
8. Eubanks, S., Nguyen, T., Peyton, D., and Breslow, E. (2000) *Biochemistry 39*, 8085−8094.
9. Marley, J., Lu, M., and Bracken, C. (2001) *J. Biomol. NMR. 20*, 71−75.
10. Marion, D., and Wuthrich, K. (1983) *Biochem. Biophys. Res. Commun. 113*, 967−974.
11. Kay, L. E., Keifer, P., and Saarinen, T. (1992) *J. Am. Chem. Soc. 114*, 10663−10665.
12. Live, D. H., Davis, D. G., Agosta, W. C., and Cowburn, D. (1984) *J. Am. Chem. Soc. 106*, 1939−1941.
13. Delaglio, F., Grzesiek, S., Vuister, G. W., Zhu, G., Pfeifer, J., and Bax, A. (1995) *J. Biomol. NMR 6*, 277−293.
14. Johnson, B. A., and Blevins, R. A. (1994) *J. Biomol. NMR 4*, 603−614.
15. Bodenhausen, G., and Ruben, D. G. (1980) *Chem. Phys. Lett. 69*, 185−189.
16. Grzesiek, S., and Bax, A. (1992) *J. Magn. Reson. 96*, 432−440.
17. Yamazaki, T.; Lee, N.; Arrowsmith, C. H.; Muhandiram, D. R.; Kay, L. E. (1994) *J. Am. Chem. Soc. 116*, 11655.
18. Wittekind, M., and Mueller, L. (1993) *J. Magn. Reson. B101*, 201−205.
19. Muhandiram, D. R., and Kay, L. E. (1994) *J. Magn. Reson. 103*, 203−216.
20. Zhang, O., Kay, L. E., Olivier, J. P., and Forman-Kay, J. D. (1994) *J. Biomol. NMR 4*, 845−858.
21. Kay, L. E., Xu, G. Y., Singer, A. U., Muhandiram, D. R., and Forman-Kay, J. D. (1993) *J. Magn. Reson. B101*, 333−337.
22. Kuboniwa, H., Grzesiek, S., Delaglio, F., and Bax, A. (1994) *J. Biomol. NMR 4*, 871−878.
23. Mayer, K. L., and Stone, M. J. (2000) *Biochemistry 39*, 8382−8395.
24. Cornilescu, G., Delaglio, F., and Bax, A. (1999) *J. Biomol. NMR 13*, 289−302.
25. Brunger, A. T., Adams, P. D., Clore, G. M., Delano, W. L., Gros, P., Grosse-Kunstleve, R. W., Jiang, J.-S., Kuszewski, J., Nilges, M., Pannu, N. S., Read, R. J., Rice, L. M., Simonson, T., and Warren, G. L. (1998) *Acta Crystallogr. D54*, 905−921.
26. Fletcher, C. M., Jones, D. N. M., Diamond, R., and Neuhaus, D. (1996) *J. Biomol. 8*, 292−310.
27. Garrett, D. S., Kuszewski, J., Hancock, T. J., Lodi, P. J., Vuister, G. W., Gronenborn, A. M., and Clore, G. M. (1994) *J. Magn. Reson. Ser. B104*, 99−103.
28. Kuszewski, J., Qin, J., Gronenborn, A. M., and Clore, G. M. (1995) *J. Magn. Reson. Ser. B106*, 92−96.
29. Kuszewski, J., Gronenborn, A. M., and Clore, G. M. NMR. (1995) *J. Magn. Reson. Ser. B107*, 293−297.
30. Qin, J., Clore, G. M., Kennedy, W. P., Kuszewski, J., and Gronenborn, A. M. (1996) *Structure 4*, 613−620.
31. Laskowski, R. A., Rullmann, J. A., MacArthur, M. W., Kaptein, R., and Thornton, J. M. (1996) *J. Biomol. NMR 8*, 477−486.
32. Koradi, R., Billeter, M., and Wuthrich, K. (1996) *J. Mol. Graphics 14*, 52−55.
33. Zheng, C., Peyton, D., and Breslow, E. (1997) *J. Peptide Res. 50*, 199−209.
34. Breslow, E., Sardana, V., Deeb, R., Barbar, E., and Peyton, D. H. (1995) *Biochemistry 34*, 2137−2147.
35. Peyton, D., Sardana, V., and Breslow, E. (1986) *Biochemistry 25*, 6579−6586.
36. Wishart, D. S., Sykes, B. D., and Richards, F. M. (1992) *Biochemistry 31*, 16478−1651.
37. Metzler, W. J., Constantine, K. L., Friedrichs, M. S., Bell, A. J., Ernst, E. G., Lavoie, T. B., and Mueller, L. (1993) *Biochemistry 32*, 13818−13829.
38. Breslow, E., Mishra, P. K., Huang, H.-B., and Bothner-by, A. (1992) *Biochemistry 31*, 11397−11404.
39. Eubanks, S., Nguyen, T. L., Deeb, R., Villafania, A., Alfadhli, A., and Breslow, E. (2001) *J. Biol. Chem. 276*, 29671−29680.
40. Zheng, C., Cahill, S., and Breslow, E. (1996) *Biochemistry 35*, 11763−11772.
41. Sardana, V., and Breslow, E. (1986) *Fed. Proc. 45*, 1538.
42. Breslow, E., LaBorde, T., Bamezai, S., and Scarlata, S. (1991) *Biochemistry 30*, 7990−8000.
43. Sardana, V., and Breslow, E. (1984) *J. Biol. Chem. 259*, 3669−3679.
44. Chauvet, M, T., Hurpet, D., Chauvet, J., and Acher, R. (1983) *Proc. Natl. Acad. Sci. U.S.A. 80*, 2839−2843.
45. Guex, N., and Peitsch, M. C. (1997) *Electrophoresis 18*, 2714−2723.

BI012067K